Supporting information

Modulating surface segregation of PdCuRu nanocrystals for enhanced all-pH hydrogen evolution electrocatalysis

Menggang Li,[ab#] Mingchuan Luo,[b#] Zhonghong Xia,[b] Yong Yang,[b] Yarong Huang,[a] Dong Wu,[b] Yingjun Sun,[b] Chunji Li,[b] Yuguang Chao,[b] Wenxiu Yang,[b] Weiwei Yang,[a]* Yongsheng Yu,[a]* and Shaojun Guo[bc]*

a MIIT Key Laboratory of Critical Materials Technology for New Energy Conversion and Storage, School of Chemistry and Chemical Engineering, Harbin Institute of Technology, Harbin, Heilongjiang 150001, China. E-mail: yangww@hit.edu.cn, ysyu@hit.edu.cn

b Department of Materials Science & Engineering, College of Engineering, Peking University, Beijing 100871, China. E-mail: guosj@pku.edu.cn

c BIC-ESAT, College of Engineering, Peking University, Beijing 100871, China

[#] These authors contributed equally to this work.

Experimental section

Chemicals. Palladium (Ⅱ) acetylacetonate ($Pd(acac)_2$, 99%) was purchased from Sigma-Aldrich. Copper (II) acetylacetonate ($Cu(acac)_2$, 97%), ruthenium (Ⅲ) acetylacetonate ($Ru(acac)_3$, 97%), commercial Pt/C (20 *wt.*%), commercial/C (10 *wt.*%), and Nafion (5 *wt.*%) were all obtained from Alfa Aesar. L-ascorbic acid (AA, AR.) and isopropyl alcohol were supplied by J&K Scientifc. Iron (Ⅲ) chloride hexahydrate ($FeCl_3 \cdot 6H_2O$, AR.), potassium dihydrogen phosphate (KH_2PO_4, AR.), di-potassium hydrogen phosphate trihydrate ($K_2HPO_4 \cdot 3H_2O$, AR.) and perchloric acid ($HClO_4$, GR., 70%-72%) were all bought from Sinopharm Chemical Reagent Co. Ltd. Potassium hydroxide (KOH, GR., 95%) and acetic acid (36%) were obtained from Aladdin. Ethanol and cyclohexane were provided by Beijing Tongguang Fine Chemicals Company. All the reagents and chemicals were used as received without purification. Besides, the ultrapure water (18.2 MΩ cm^{-1}) used in all experiments was prepared by passing through an ultra-pure purification system.

Synthesis of PdCuRu nanocrystals. In a typical synthesis of $Pd_{45}Cu_{39}Ru_{16}$ nanocrystals, $Pd(acac)_2$ (0.025 mmol), $Cu(acac)_2$ (0.05 mmol), $Ru(acac)_3$ (0.0175 mmol), $FeCl_3 \cdot 6H_2O$ (0.02 mmol), AA (0.2 mmol), and OAm (5mL) were put in a sealed vial (volume: 20 mL). The mixture was ultrasonicated for 1.0 h to obtain a transparent solution. The vial was then transferred into an oil bath at a temperature of 180 ºC, and maintained this temperature for 12 h before being cooling down to room temperature. The resulting black colloidal products were collected by centrifugation with an ethanol/cyclohexane mixture, and then dispersed in 8 mL cyclohexane for further use. $Pd_{50}Cu_{50}$ nanocrystals were obtained by using the similar procedure except for the absence of Ru precursors. PdCuRu nanocrystals with different compositions could be prepared by changing the amount of $Ru(acac)_3$ to 0.006 mmol, 0.0125 mmol, 0.025 mmol, and 0.05 mmol, respectively, and keep the other reaction conditions unchanged.

Preparation of PdCuRu/C. The obtained nanocrystals dispersed in cyclohexane (8 mL) and Ketjen Black-300 J carbon supports (15 mg) dispersed in ethanol (50mL) were mixed under sonication for 3 h, and then the black products were collected by centrifugation. The remained organic impurities on nanocrystals were removed by being subject to heating at 60 °C in acetic acid (36%) for 2 h under N_2 atmosphere. The products were separated by centrifugation and washed with ethanol for several times and dried at 60 °C for the next step.

Preparation of $Pd_{45}Cu_{39}Ru_{16}$/C-350, $Pd_{45}Cu_{39}Ru_{16}$/C-400, $Pd_{45}Cu_{39}Ru_{16}$/C-450, $Pd_{45}Cu_{39}Ru_{16}$/C-500. The as-prepared $Pd_{45}Cu_{39}Ru_{16}$/C was annealed at 350 °C, 400 °C, 450 °C, and 500 °C under a 5% H_2/95% Ar for 1 h with a heating rate of 5 °C min^{-1}, respectively. The final samples were denoted as $Pd_{45}Cu_{39}Ru_{16}$/C-350, $Pd_{45}Cu_{39}Ru_{16}$/C-400, $Pd_{45}Cu_{39}Ru_{16}$/C-450, and $Pd_{45}Cu_{39}Ru_{16}$/C-500, respectively.

Characterization. Transmission electron microscopy (TEM) images were conducted on a HITACHI H-7700 transmission electron microscopy with an accelerating voltage of 100 kV and the high resolution TEM (HRTEM) images were obtained on a FEI Tecnai-G2 F30 at an accelerating voltage of 300 kV. Scanning electron microscopy-energy dispersive X-ray spectroscopy (SEM-EDS) spectra were performed on a JEOL JSM-6360 scanning electron microscope with an accelerating voltage of 200 kV. X-ray diffraction (XRD) patterns were collected on a PANalytical-XRD instrument using Cu Kα radiation X-ray source (λ = 0.15406 nm) at the voltage of 40 kV as well as the current of 30 mA. Inductively coupled plasma atomic emission spectrometry (ICP-AES) analysis was determined using an Agilent 8800 instrument. X-ray photoelectron spectroscopy (XPS) tests were carried out with Thermo Scientifc Escalab 250Xi using a monochromated Al-Kα (1486.5 eV) X-ray radiation.

Electrochemical measurements. The obtained catalysts were dispersed and sonicated in a mixture of isopropyl alcohol, ultrapure water and Nafion solution (volume ratio is 1 : 1 : 0.008) to form a homogeneous ink (1 mg mL^{-1}). A 1 mg mL^{-1} ink of Pt/C (JM, 20 *wt.*%) was prepared and a 2 mg mL^{-1} ink of Pd/C (JM, 10 *wt.*%) was also prepared. Then, 10 μL of the mixture ink was deposited on a polished glassy carbon (GC) working electrode (5 mm, 0.196 cm^2) and dried at ambient conditions.

The electrochemical tests were measured in alkaline (0.1 M KOH), neutral (0.5 M PBS), and acidic (0.1 M $HClO_4$) solutions on a CHI 660e electrochemical workstation (CH Instruments, *Inc.*, Shanghai) with a typical three-electrode system, consisting of a GC working electrode (Pine Instruments, 5 mm of diameter), saturated calomel electrode (SCE), and carbon rod served as the working, reference and counter electrodes, respectively. Before measurements, the electrolyte was bubbling by N_2 for at least 30 minutes to remove residual O_2. The polarization curves were tested at a scan rate of 5 mV s^{-1}, and obtained with 95% iR compensations. All recorded related potentials were converted to the reversible hydrogen electrode (RHE).

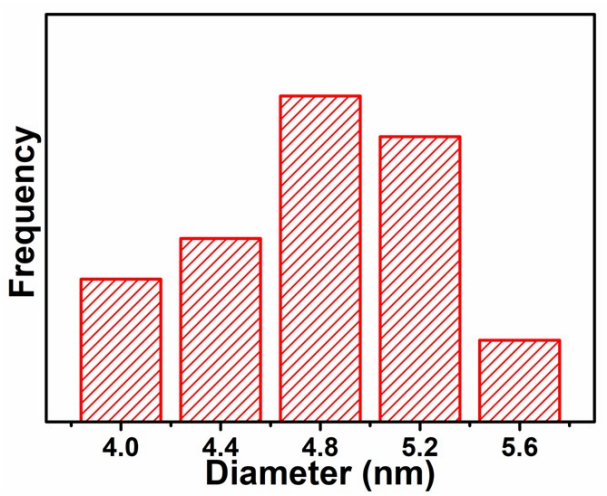

Figure S1. The size distribution of $Pd_{25}Cu_{56}Ru_{14}$ nanocrystals.

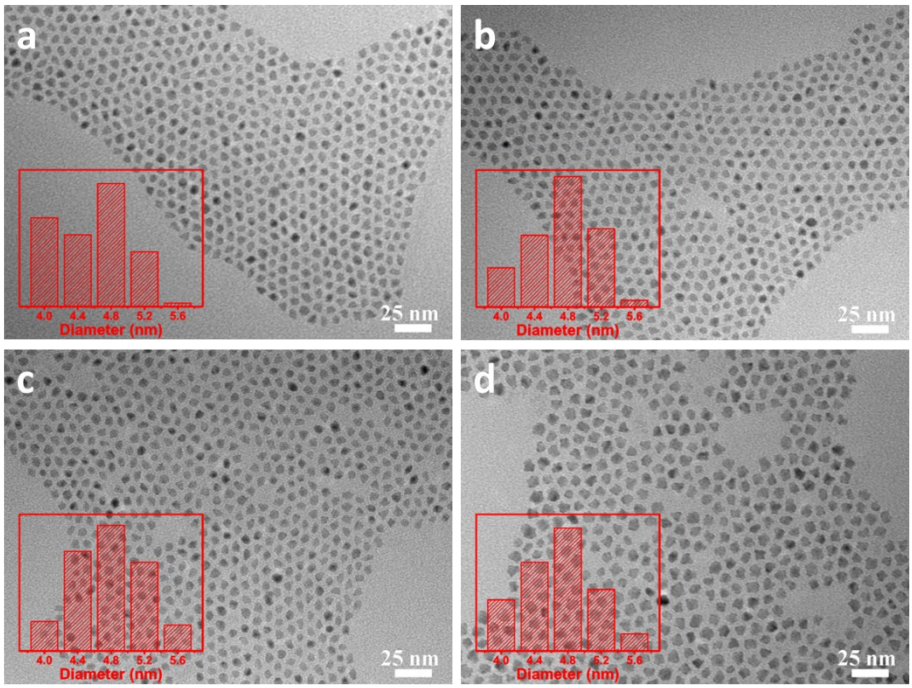

Figure S2. The representative TEM images of (a) $Pd_{32}Cu_{59}Ru_9$, (b) $Pd_{29}Cu_{58}Ru_{13}$, (c) $Pd_{27}Cu_{55}Ru_{17}$ and (d) $Pd_{23}Cu_{51}Ru_{26}$ nanocrystals (the *insets* are the corresponding size distributions).

.

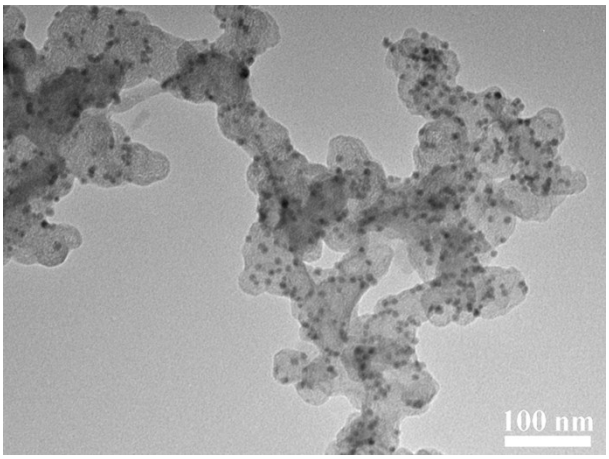

Figure S3. The representative TEM image of $Pd_{45}Cu_{39}Ru_{16}/C$.

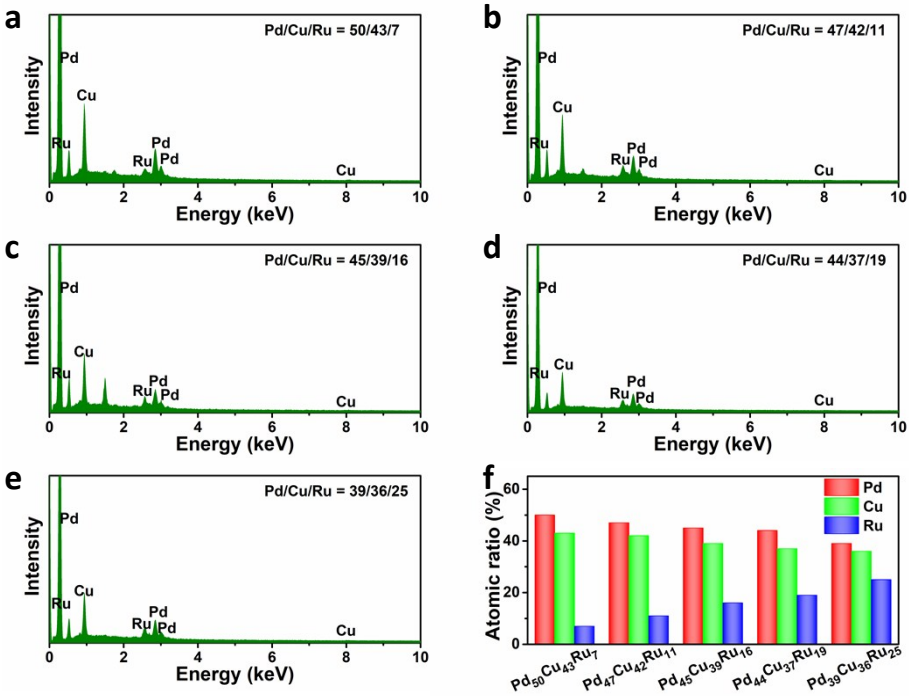

Figure S4. The SEM-EDS spectra of (a) $Pd_{50}Cu_{43}Ru_7/C$, (b) $Pd_{47}Cu_{42}Ru_{11}/C$, (c) $Pd_{45}Cu_{39}Ru_{16}/C$, (d) $Pd_{44}Cu_{37}Ru_{19}/C$ and (e) $Pd_{39}Cu_{36}Ru_{25}/C$ nanocrystals. (f) The ICP-OES results of PdCuRu/C with different atomic ratios.

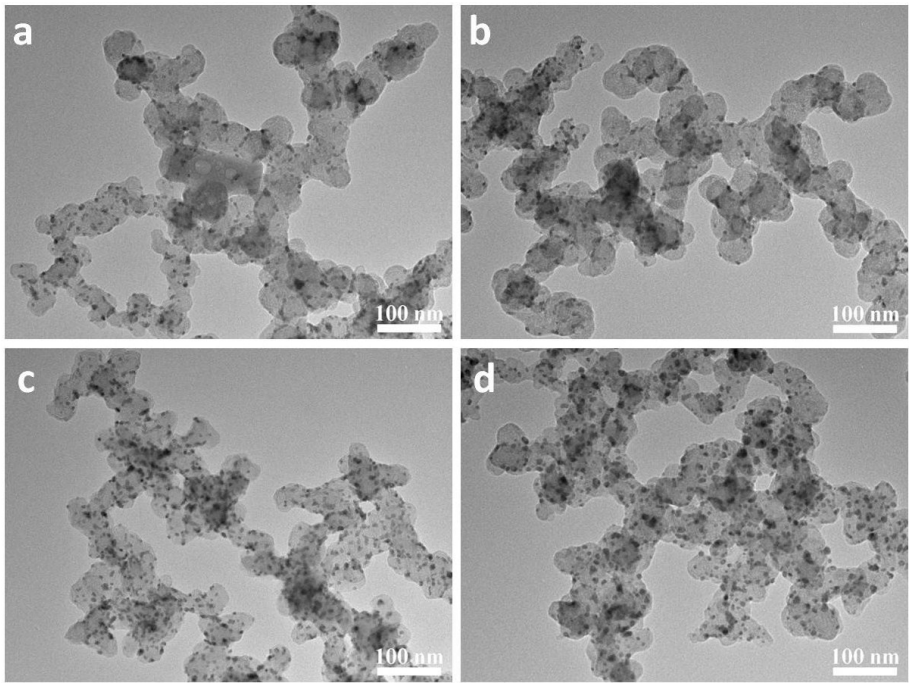

Figure S5. The representative TEM images of (a) $Pd_{45}Cu_{39}Ru_{16}$/C-350, (b) $Pd_{45}Cu_{39}Ru_{16}$/C-400, (c) $Pd_{45}Cu_{39}Ru_{16}$/C-500 and (d) $Pd_{45}Cu_{39}Ru_{16}$/C-500.

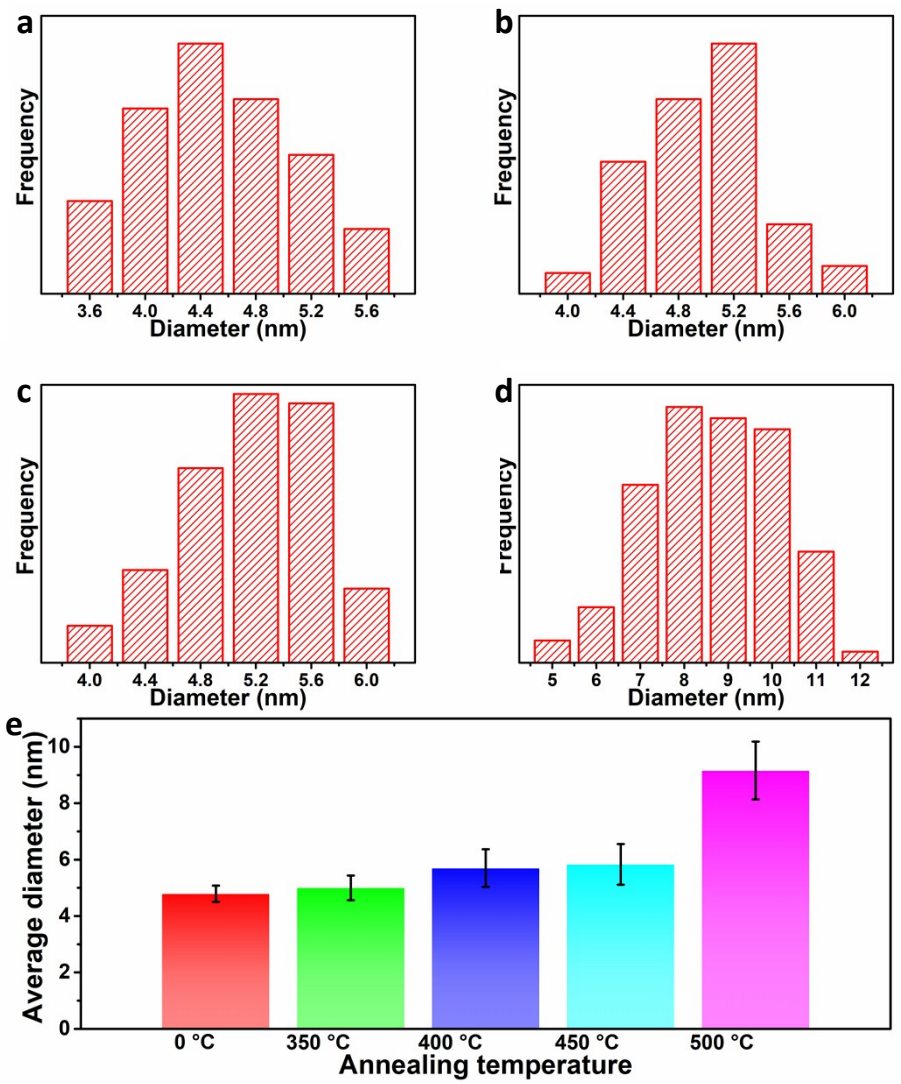

Figure S6. The size distributions of (a) $Pd_{45}Cu_{39}Ru_{16}$/C-350, (b) $Pd_{45}Cu_{39}Ru_{16}$/C-400, (c) $Pd_{45}Cu_{39}Ru_{16}$/C-450 and (d) $Pd_{45}Cu_{39}Ru_{16}$/C-500. (e) The average diameter of $Pd_{45}Cu_{39}Ru_{16}$/C with different annealing temperature.

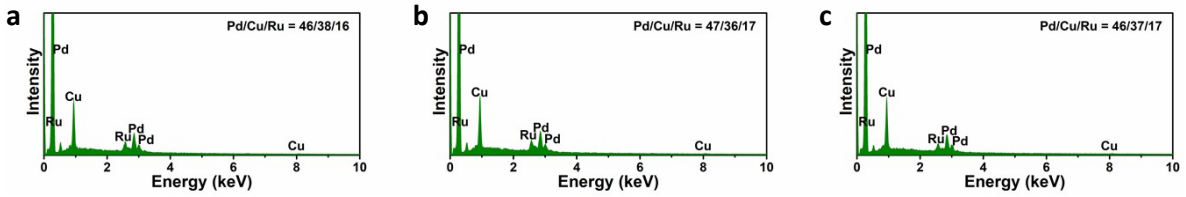

Figure S7. The SEM-EDS spectra of (a) $Pd_{45}Cu_{39}Ru_{16}$/C-350, (b) $Pd_{45}Cu_{39}Ru_{16}$/C-400, and (c) $Pd_{45}Cu_{39}Ru_{16}$/C -500.

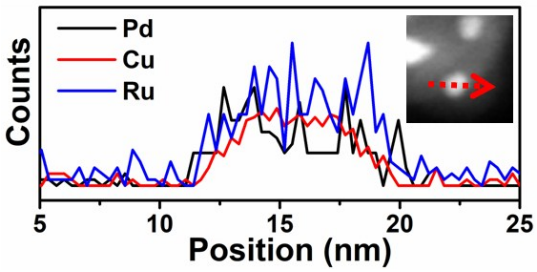

Figure S8. Elemental line-scan analysis across the red arrow in the *inset* of the single $Pd_{45}Cu_{39}Ru_{16}$ nanocrystal.

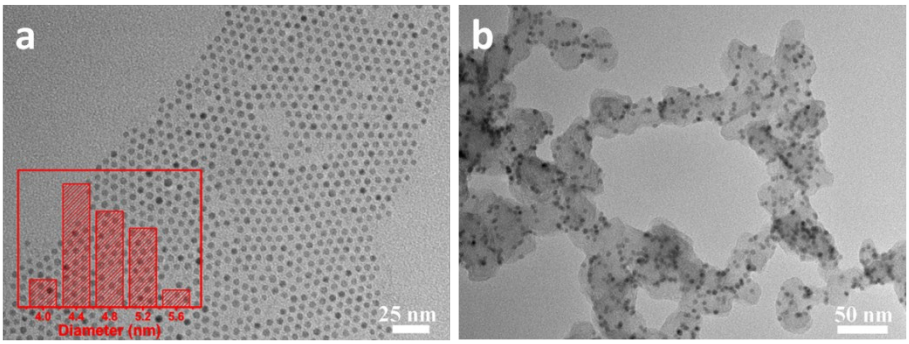

Figure S9. (a) The representative TEM image of $Pd_{50}Cu_{50}$ nanocrystals (the *inset* is the corresponding size distribution). (b) The representative TEM image of $Pd_{50}Cu_{50}$/C.

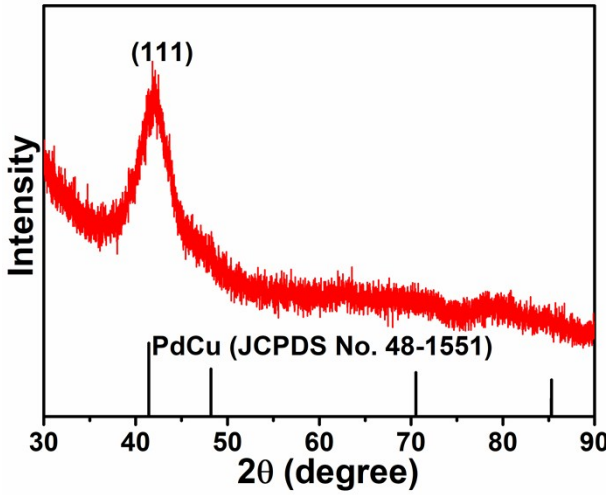

Figure S10. XRD pattern of $Pd_{50}Cu_{50}$/C.

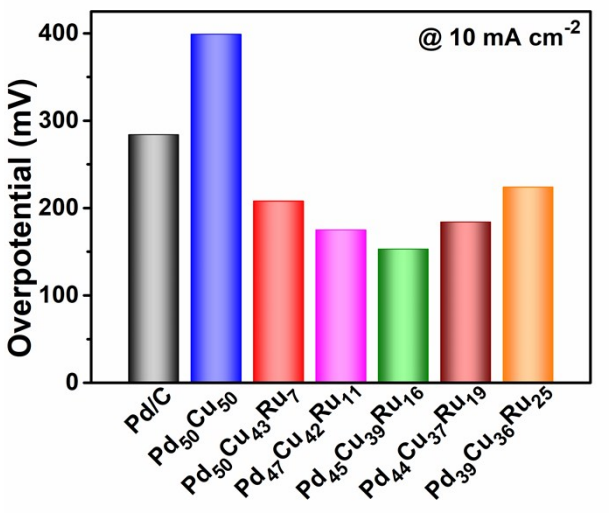

Figure S11. (a) Overpotentials at a current density of 10 mA cm^{-2}, and (b) Tafel slopes of PdCuRu/C with different compositions and the commercial Pd/C electrocatalysts.

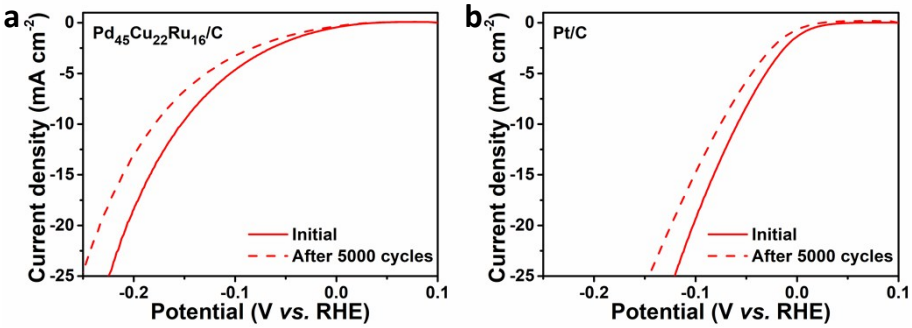

Figure S12. The polarization curves of (a) $Pd_{45}Cu_{39}Ru_{16}$/C and (b) commercial Pt/C before and after 5000 potential cycles in 0.1 M KOH.

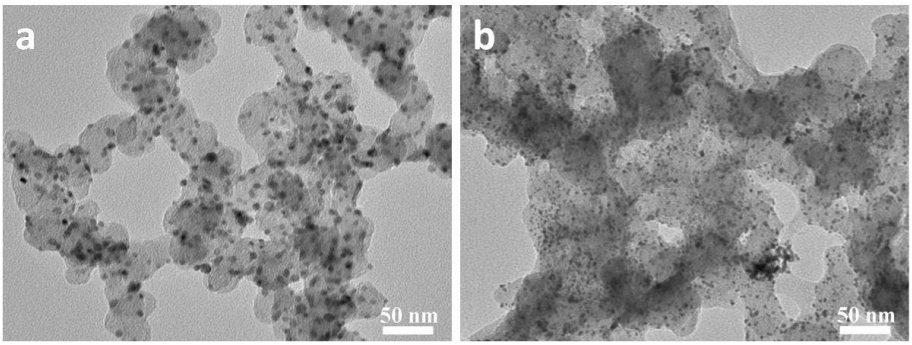

Figure S13. The representative TEM images of (a) $Pd_{45}Cu_{39}Ru_{16}$/C and (b) commercial Pt/C after 5000 cycles.

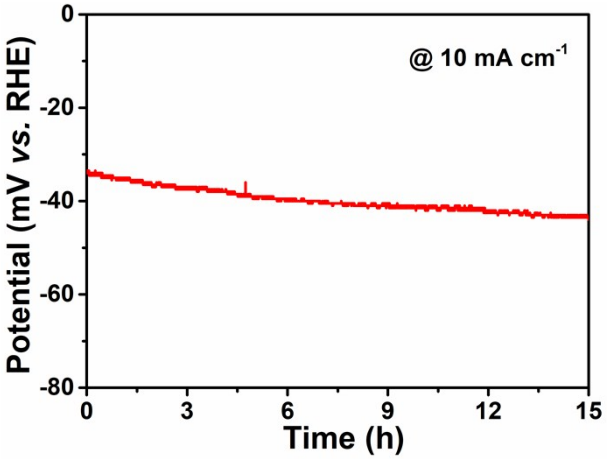

Figure S14. The chronopotentiometry measurement at a current density of 10 mA cm^{-2} of $Pd_{45}Cu_{39}Ru_{16}$/C-450 in 0.1 M KOH.

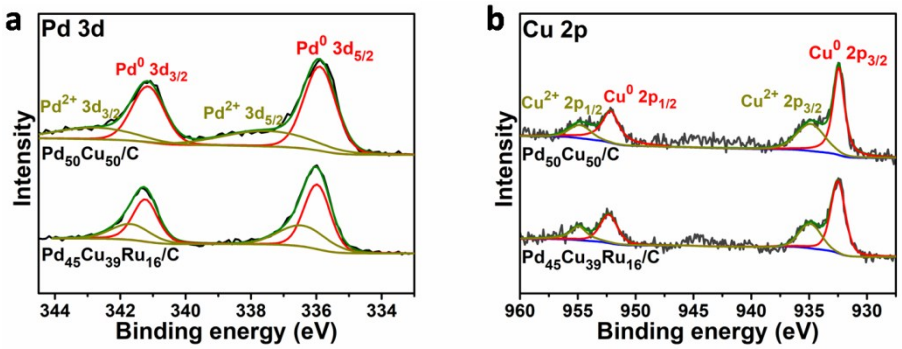

Figure S15. The XPS spectra and deconvoluted peaks of $Pd_{50}Cu_{50}$/C and $Pd_{45}Cu_{39}Ru_{16}$/C in regions of (a) Pd 3d and (b) Cu 2p.

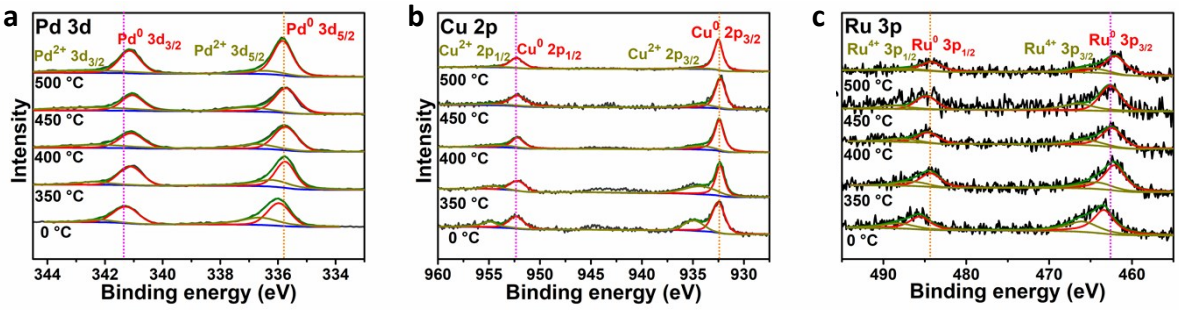

Figure S16. The XPS spectra and deconvoluted peaks of $Pd_{45}Cu_{39}Ru_{16}$/C with different annealing temperatures under H_2/Ar atmosphere in regions of (a) Pd 3d, (b) Cu 2p and (c) Ru 3p.

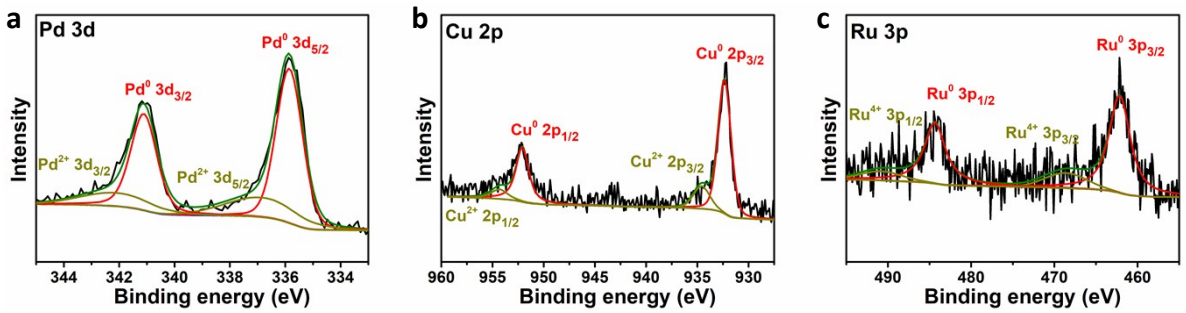

Figure S17. The XPS spectra and deconvoluted peaks of $Pd_{45}Cu_{39}Ru_{16}$/C after HER durability test in regions of (a) Pd 3d, (b) Cu 2p and (c) Ru 3p.

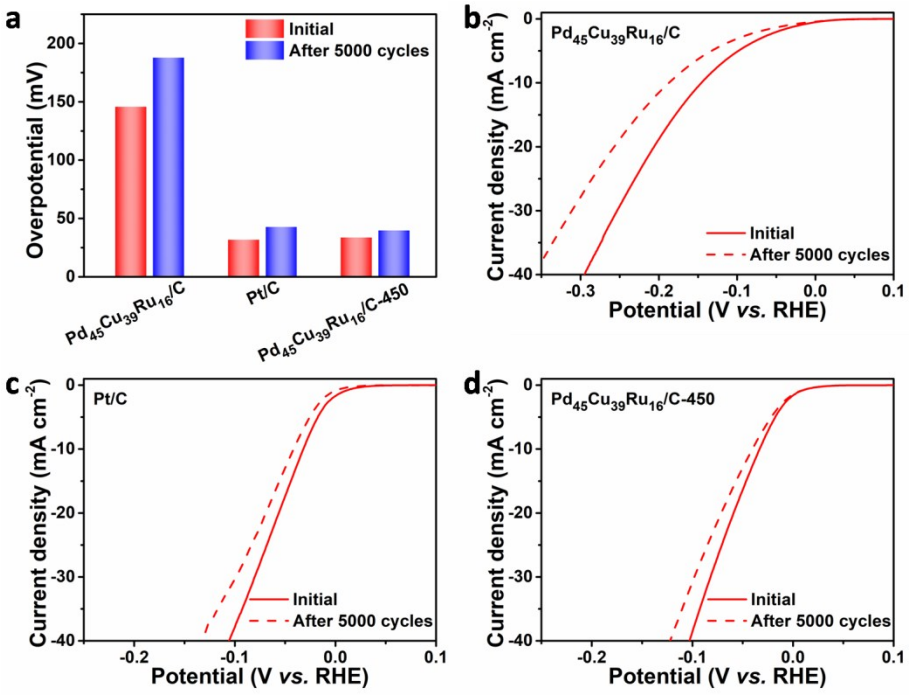

Figure S18. (a) The electrochemical stability of different catalysts after 5000 potential cycles in 0.5 M PBS. The polarization curves of (b) $Pd_{45}Cu_{39}Ru_{16}$/C, (c) commercial Pt/C and (d) $Pd_{45}Cu_{39}Ru_{16}$/C-450 before and after 5000 potential cycles in 0.5 M PBS.

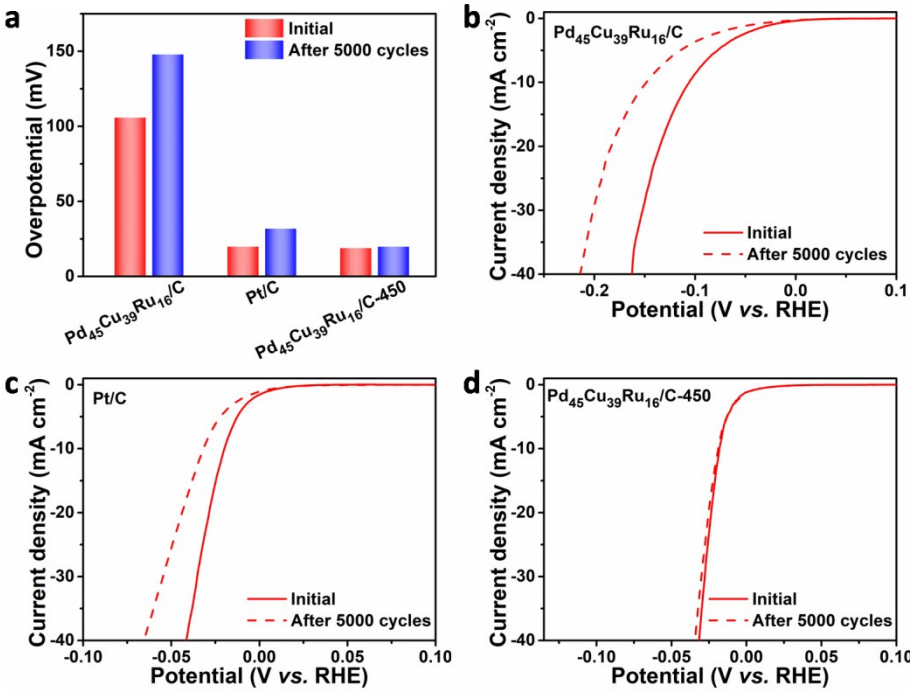

Figure S19. (a) The electrochemical stability of different catalysts after 5000 potential cycles in 0.1 M $HClO_4$. The polarization curves of (b) $Pd_{45}Cu_{39}Ru_{16}$/C, (c) commercial Pt/C and (d) $Pd_{45}Cu_{39}Ru_{16}$/C-450 before and after 5000 potential cycles in 0.1 M $HClO_4$.

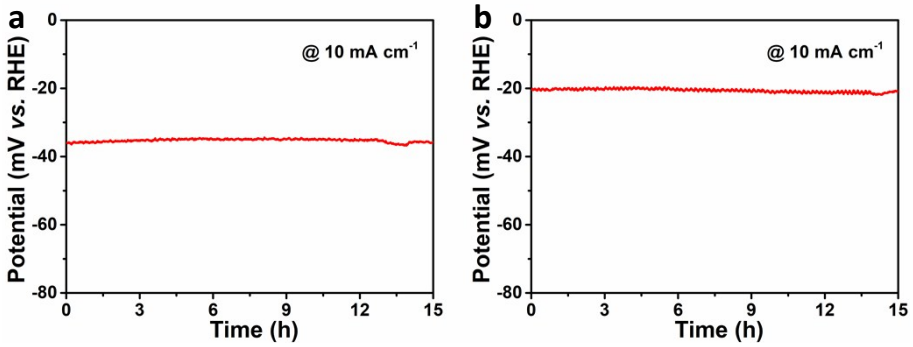

Figure S20. The chronopotentiometry measurements at a current density of 10 mA cm^{-2} of $Pd_{45}Cu_{39}Ru_{16}$/C-450 in (a) 0.5 M PBS and (b) 0.1 M $HClO_4$.

Table S1. The composition percentage of different atomics of $Pd_{45}Cu_{39}Ru_{16}$/C electrocatalysts treated with different annealing temperatures obtained from XPS and ICP-OES results.

Catalysts	XPS (%)			ICP-OES (%)		
	Pd	Cu	Ru	Pd	Cu	Ru
$Pd_{45}Cu_{39}Ru_{16}$/C	33.5	28.7	37.8	45.5	38.6	15.9
$Pd_{45}Cu_{39}Ru_{16}$/C-350	41.0	25.3	33.7	46.1	38.1	15.8
$Pd_{45}Cu_{39}Ru_{16}$/C-300	47.3	24.2	28.5	47.1	35.6	17.3
$Pd_{45}Cu_{39}Ru_{16}$/C-450	56.1	23.8	20.1	46.4	34.9	18.7
$Pd_{45}Cu_{39}Ru_{16}$/C-500	56.4	24.4	19.2	45.8	36.6	17.6

Table S2. Comparison of HER catalytic performance in alkaline/neutral/acid media for $Pd_{45}Cu_{39}Ru_{16}$/C-450 with other reported HER electrocatalysts.

Catalysts	Overpotential@*j* ($mV@10\ mA\ cm^{-2}$)	Tafel slopes ($mV\ dec^{-1}$)	Electrolytes	References
$Pd_{45}Cu_{39}Ru_{16}$/C-450	31	52	0.1 M KOH	This work
	34	39	0.5 M PBS	
	19	22	0.1 M $HClO_4$	
PdCu nanosheets	106	123	1.0 M KOH	[1]
PdCu nanoparticles	75	48	0.1 M H_2SO_4	[2]
PdCu@Pd nanocubes	68	35	0.5 M H_2SO_4	[3]
Pd/Cu-Pt nanorings	22.8	25	0.5 M H_2SO_4	[4]
$PdCu_3$ nanoparticles	50	34	0.5 M H_2SO_4	[5]
PdNiMo film	110	227	1.0 M NaOH	[6]
PdTe nanowires	97	90	1.0 M KOH	[7]
	48	63	0.5 M H_2SO_4	

$Pd_{17}Se$ films	182	57		
Pd_7Se films	162	56	0.5 M H_2SO_4	[8]
Pd_4Se films	94	50		
Pd nanoparticles/CN_X	55	35	0.5 M H_2SO_4	[9]
PdCo alloy	80	31	0.5 M H_2SO_4	[10]
	250	NA	1.0 M KOH	
PdMnCo alloy	39	31	0.5 M H_2SO_4	[11]
Pt_2Pd/NPG	58	31	0.5 M H_2SO_4	[12]
Pt@Pd nanoflowers	56	39	0.5 M H_2SO_4	[13]
$Ru/C_3N_4/C$	79	69	0.1 M KOH	[14]
Ru nanodendrites	43.4	49	1.0 M KOH	[15]
RuNi nanoplates	39.3	25	0.1 M KOH	[16]
	40	23.4	1.0 M KOH	
Ru@CN	32	53	1.0 M KOH	[17]
	100	NA	1.0 M PBS	
	126	NA	0.5 M H_2SO_4	
Ru_2P nanoparticles	52	69	1.0 M KOH	[18]
	57	87	1.0 M PBS	
	38	38	0.5 M H_2SO_4	
Ru@NiCoP	52	50	1.0 M KOH	[19]
	49	49	0.5 M H_2SO_4	
Thick hollow	82	48	1.0 M KOH	[20]

$Cu_{2-x}S$@Ru NPs	129	51	0.5 M H_2SO_4	
Ru/GLC	35	46	0.5 M H_2SO_4	[21]
PtRu nanoclusters	21.6	27.2	0.5 M H_2SO_4	[22]

NA: Not available

Table S3. The valence state ratios of Pd^0/Pd^{2+}, Cu^0/Cu^{2+}, and Ru^0/Ru^{4+}obtained from XPS spectra of $Pd_{45}Cu_{39}Ru_{16}$/C electrocatalysts treated with different annealing temperatures.

Catalysts	Pd^0/Pd^{2+}	Cu^0/Cu^{2+}	Ru^0/Ru^{4+}
$Pd_{45}Cu_{39}Ru_{16}$/C	1.81	2.11	1.58
$Pd_{45}Cu_{39}Ru_{16}$/C-350	2.08	2.30	2.59
$Pd_{45}Cu_{39}Ru_{16}$/C-300	2.12	3.29	2.74
$Pd_{45}Cu_{39}Ru_{16}$/C-450	2.33	3.47	3.16
$Pd_{45}Cu_{39}Ru_{16}$/C-500	2.77	17.40	3.67
$Pd_{45}Cu_{39}Ru_{16}$/C-450 (After HER tests)	3.03	4.72	4.49

Table S4. Summary of binding energies of $Pd_{45}Cu_{39}Ru_{16}$/C electrocatalysts treated with different annealing temperatures from XPS results, including Pd^0 $3d_{5/2}$, Cu^0 $2p_{3/2}$ and Ru^0 $3p_{3/2}$ states.

Catalysts	Pd^0 $3d_{5/2}$	Cu^0 $2p_{3/2}$	Ru^0 $3p_{3/2}$
$Pd_{45}Cu_{39}Ru_{16}$/C (eV)	335.97	932.54	463.38
$Pd_{45}Cu_{39}Ru_{16}$/C-350 (eV)	335.81	932.39	462.09
$Pd_{45}Cu_{39}Ru_{16}$/C-400 (eV)	335.78	932.42	462.38
$Pd_{45}Cu_{39}Ru_{16}$/C-450 (eV)	335.75	932.37	462.63
$Pd_{45}Cu_{39}Ru_{16}$/C-500 (eV)	335.84	932.52	461.98
$Pd_{45}Cu_{39}Ru_{16}$/C-450 (After HER tests) (eV)	335.84	932.34	462.15

References

1 X. Zhao, L. Dai, Q. Qin, F. Pei, C. Hu and N. Zheng, *Small*, 2017, **13**, 1602970.

2 X. Zhang, D. Wu and D. Cheng, *Electrochim. Acta*, 2017, **246**, 572-579.

3 J. Li, F. Li, S. X. Guo, J. Zhang and J. Ma, *ACS Appl. Mater. Interfaces*, 2017, **9**, 8151-8160.

4 T. Chao, X. Luo, W. Chen, B. Jiang, J. Ge, Y. Lin, G. Wu, X. Wang, Y. Hu, Z. Zhuang, Y. Wu, X. Hong and Y. Li, *Angew. Chem. Int. Ed.*, 2017, **56**, 16047-16051.

5 R. Jana, A. Bhim, P. Bothra, S. K. Pati and S. C. Peter, *ChemSusChem*, 2016, **9**, 2922-2927.

6 J. Tang, X. Zhao, Y. Zuo, P. Ju and Y. Tang, *Electrochim. Acta*, 2015, **174**, 1041-1049.

7 L. Jiao, F. Li, X. Li, R. Ren, J. Li, X. Zhou, J. Jin and R. Li, *Nanoscale*, 2015, **7**, 18441-18445.

8 S. Kukunuri, P. M. Austeria and S. Sampath, *Chem. Commun.*, 2016, **52**, 206-209.

9 T. Bhowmik, M. K. Kundu and S. Barman, *ACS Catal.*, 2016, **6**, 1929-1941.

10 J. Chen, G. Xia, P. Jiang, Y. Yang, R. Li, R. Shi, J. Su and Q. Chen, *ACS Appl. Mater. Interfaces*, 2016, **8**, 13378-13383.

11 R. Zhang, Z. Sun, R. Feng, Z. Lin, H. Liu, M. Li, Y. Yang, R. Shi, W. Zhang and Q. Chen, *ACS Appl. Mater. Interfaces*, 2017, **9**, 38419-38427.

12 X. Zhong, Y. Qin, X. Chen, W. Xu, G. Zhuang, X. Li and J. Wang, *Carbon*, 2017, **114**, 740-748.

13 X. X. Lin, A. J. Wang, K. M. Fang, J. Yuan and J. J. Feng, *ACS Sustainable Chem. Eng.*, 2017, **5**, 8675-8683.

14 Y. Zheng, Y. Jiao, Y. Zhu, L. H. Li, Y. Han, Y. Chen, M. Jaroniec and S. Z. Qiao, *J. Am. Chem. Soc.*, 2016, **138**, 16174-16181.

15 K. Gao, Y. Wang, Z. Wang, Z. Zhu, J. Wang, Z. Luo, C. Zhang, X. Huang, H. Zhang and W. Huang, *Chem. Commun.*, 2018, **54**, 4613-4616.

16 J. Ding, Q. Shao, Y. Feng and X. Huang, *Nano Energy*, 2018, **47**, 1-7.

17 J. Wang, Z. Wei, S. Mao, H. Li and Y. Wang, *Energy Environ. Sci.*, 2018, **11**, 800-806.

18 Z. Pu, I. S. Amiinu, Z. Kou, W. Li and S. Mu, *Angew. Chem. Int. Ed.*, 2017, **56**, 11559-11564.

19 S. Liu, Q. Liu, Y. Lv, B. Chen, Q. Zhou, L. Wang, Q. Zheng, C. Che and C. Chen, *Chem. Commun.*, 2017, **53**, 13153-13156.

20 D. Yoon, J. Lee, B. Seo, B. Kim, H. Baik, S. H. Joo and K. Lee, *Small*, 2017, **13**, 1700052.

21 Z. Chen, J. Lu, Y. Ai, Y. Ji, T. Adschiri and L. Wan, *ACS Appl. Mater. Interfaces*, 2016, **8**, 35132-35137.

22 K. Li, Y. Li, Y. Wang, J. Ge, C. Liu and W. Xing, *Energy Environ. Sci.*, 2018, **11**, 1232-1239.